International Journal of Engineering, Science and Information Technology
Volume 5, No. 3 (2025) pp. 456-463
eISSN: 2775-2674
Website: http://ijesty.org/index.php/ijesty
DOI: https://doi.org/10.52088/ijesty.v5i3.1086
Research Paper, Short Communication, Review, Technical Paper

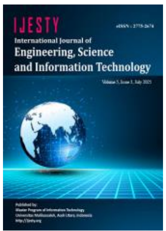

The Mechanical Properties of Bismuth-based Ceramic Nanocomposite

Nurmalita Nurmalita[1], Ahmad Fikri[1], Masrullita Masrullita[2], Novi Sylvia[2], Zetta Fazira[3], Jalaluddin[2], Zainuddin Ginting[2*]

[1]Department of Material Engineering, Universitas Malikussaleh, Aceh, Indonesia
[2]Department of Chemical Engineering, Universitas Malikussaleh, Aceh, Indonesia
[3]Department of Chemical Engineering, Politeknik Negeri Lhokseumawe, Aceh, Indonesia

**Corresponding author Email: zginting@unimal.ac.id*

The manuscript was received on 17 January 2025, revised on 15 June 2025, and accepted on 8 July 2025, date of publication 9 July 2025

Abstract

This research investigated a Bismuth-based ceramic nanocomposite material with the stoichiometric composition $Bi_{1.6}Pb_{0.4}Sr_2Ca_2Cu_3O$_y (abbreviated as B(P)SCCO-2223), synthesized via the solid-state reaction method. The fabrication process involved compound composition calculations and powder metallurgy using several high-purity oxide precursors, with bismuth oxide as the primary component. Heat treatment in the form of sintering was conducted at 846 °C for durations of 32 and 34 hours to examine its effects on the material's physical properties. Scanning Electron Microscopy (SEM) analysis revealed layered grain structures with the presence of pores at grain boundaries. Energy Dispersive X-ray (EDX) analysis confirmed that the target 2:2:2:3 elemental ratio was achieved across all samples. X-ray Diffraction (XRD) analysis showed that the sample sintered for 34 hours exhibited the largest grain size of 48.07 nm. The holding time of 34 hours during the sintering process has provided sufficient opportunity for the crystal grains to grow larger. Scanning electron microscopy photos also show that longer sintering times make the empty space between the grains smaller because the crystal grains are closer together, followed by the pore size becoming smaller. This sample also demonstrated the highest oriented phase percentage (58.12%) and the lowest impurity level (6.05%). Mechanical properties, evaluated using Vickers microhardness testing, indicated that the 34-hour sintered sample had superior performance, with a Vickers hardness of 0.925 GPa, Young's modulus of 75.813 GPa, yield strength of 0.308 GPa, fracture toughness of 5.2, surface energy of 0.178 J, and a brittleness index of 0.177. Overall, the study concluded that the physical properties of the ceramic nanocomposite improved with increased sintering duration.

Keywords: *Powder Metallurgy, Young's Modulus, Microhardness Vickers, Ceramic Nanocomposite.*

1. Introduction

Bismuth-based ceramic composites, first discovered by Maeda et al. [1], are materials capable of conducting electricity without resistance at cryogenic temperatures. These materials, commonly referred to as BSCCO, possess a layered crystal structure and exist in three distinct phases depending on their chemical composition: the Bi-2201 phase ($n = 1$, $T_c \approx 20$ K), the Bi-2212 phase ($n = 2$, $T_c \approx 85$ K), and the (Bi, Pb)-2223 phase ($n = 3$, $T_c \approx 110$ K) [2]. Among these, the (Bi, Pb)-2223 phase exhibits superior properties due to its relatively high critical temperature.

Despite their potential for use in current transmission applications—particularly in the form of long wires and ribbons—the practical implementation of BSCCO ceramics remains limited. This is primarily due to their inherent layered crystal structure, short coherence length, anisotropy, low charge carrier concentration, and weak mechanical bonding strength [3]. Nonetheless, the application era of BSCCO-based materials in superconductor cables began in 2004 [4], and since then, extensive research has been devoted to improving their physical and mechanical properties. Enhancements in the characteristics of these materials are strongly influenced by factors such as dopant type, fabrication methods, heat treatment conditions, and oxygen content [5].

As a material intended for power transmission cables, BSCCO ceramics are subjected to mechanical deformation processes, including drawing, rolling, and pressing. Therefore, ongoing research seeks to optimize fabrication conditions, reduce the formation of detrimental microcracks, and enhance the structural reliability of BSCCO ceramic composites. Previous studies have explored the mechanical enhancement of BSCCO through the incorporation of various dopants. Among them, lead (Pb) doping has been found to not only improve the mechanical strength but also raise the critical temperature of BSCCO. The substitution of Pb atoms for Bi atoms enhances the material's performance for power transmission applications [6]. In addition to doping, the optimization of heat treatment parameters—particularly sintering duration—plays a significant role in refining the microstructure, thereby contributing to improved mechanical behavior [7]. The aim of this study was to synthesize Pb-doped Bismuth-based ceramic composites using the powder metallurgy method with varied sintering durations of 32 and 34 hours. The resulting samples are evaluated based on their physical properties through X-ray diffraction (XRD), scanning electron microscopy (SEM), energy-dispersive X-ray spectroscopy (EDX), and Vickers microhardness testing.

2. Literature Review

2.1. The Vickers Microhardness

Mechanical properties such as strength, crack resistance, ductility, and hardness are critical for the industrial application of BSCCO ceramic composite materials [8]. Hardness is commonly defined as a material's resistance to scratching, cutting, abrasion, or indentation. It can also be described as the material's resistance to plastic deformation or dislocation motion [9]. Additionally, hardness reflects a material's ability to resist penetration or applied load. In microhardness testing using the Vickers method, a diamond indenter with a square-based pyramidal shape and an apex angle of α = 136° is pressed onto the surface of the specimen under a specific load (F) for a fixed duration [10]. Fig 1 illustrates a schematic diagram of the Vickers indenter and the resulting indentation marks on the material surface.

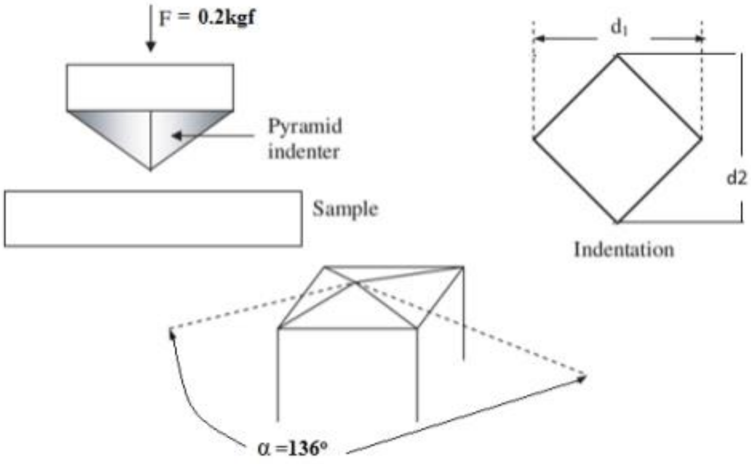

Fig 1. Schematic image of the Vickers indenter used to test microhardness

The Vickers microhardness (HV) is calculated as the ratio between the applied load (F) and the surface area of the indentation left by the diamond indenter on the specimen surface. The diagonal length (d) refers to the average of the two diagonals of the indentation impression. The fundamental formula for Vickers hardness is expressed as follows [11]:

a. Hardness (Vickers number)

$$Hv = \frac{1.854\ x\ F}{d^2} \tag{1}$$

b. Young's Modulus

$$\epsilon = 81.96\, Hv \tag{2}$$

c. Yield Strength

$$Y = \frac{Hv}{3} \tag{3}$$

d. Fracture Toughness

$$K_{IC} = \alpha \left(\frac{\epsilon}{Hv}\right)^{1/2} \cdot \frac{F}{\sqrt{r^3}} \tag{4}$$

e. Surface Energy

$$\gamma = \frac{{K_{IC}}^2}{2\epsilon} \tag{5}$$

f. Brittleness Index

$$B^I = \frac{Hv}{K_{IC}} \tag{6}$$

Where:

Hv = Hardness value according to the Vickers method (kg/mm2)
F = Load (kgf)
d = Average diagonal length (mm)
ϵ = Young's modulus
Y = Yield strength
α = constant 0.016
r = crack length (mm)
K_{IC} = Fracture toughness
γ = Surface energy

B^I = Brittleness index

2.2. The Microstructure

Microstructure at the grain level has a strong influence on the mechanical properties of the material. Therefore, XRD pattern testing of material samples can provide the required information. Based on the XRD pattern analysis, the characterization of the crystallinity of the compounds formed, volume fraction, crystal planes oriented on the c axis, crystal grain size and impurities can be determined. To observe phase growth, the volume fraction is calculated based on the XRD spectrum using the following equation [12]:

a. Volume fraction

$$Fv = \frac{\sum I\,(2223)}{I\,(Total)}\, x\ 100\% \tag{7}$$

b. Oriented phase

$$P = \frac{\sum I\,(00l)}{I\,(2223)}\, x\ 100 \tag{8}$$

c. Grain size

$$D = \frac{k\lambda}{\beta cos\theta} \tag{9}$$

d. Impurity

$$I = 100\% - FV \tag{10}$$

Where:

FV = volume fraction (%)
P = oriented phase (%)
I(2223) = phase diffraction peak intensity
I(total) = intensity of all diffraction peaks
I(00*l*) = phase diffraction peak intensity with even number *l*
D = crystal grain size (nm)
k = a constant value of 0.70 to 1.70
λ = X-ray diffraction source wavelength (Å)
β = half width of the maximum diffraction peak (FWHM)
θ = angle of difraction
I = impurity (%)

It is also known that the addition of solutes to metals and ceramics can increase mechanical strength. This is because dislocation motion can often be inhibited by the solute atoms themselves and the lattice defects created to compensate for the charge of the aliovalent dopant. If the solute concentration exceeds the solubility limit, precipitates can form which are also effective in inhibiting dislocation movement. Therefore, the addition of dopants can increase the mechanical strength of ceramics through dissolved solution mechanisms and precipitation hardening [13] .

3. Method

All samples were synthesized using the solid-state reaction method, with lead (Pb) as the dopant. The starting powders—Bi_2O_3, PbO, $SrCO_3$, CuO, and $CaCO_3$—were weighed based on powder metallurgy calculations to achieve the stoichiometric composition of $Bi_{1.6}Pb_{0.4}Sr_2Ca_2Cu_3Oy$. The materials and equipment used in this study are summarized in Table 1.

Table 1. The materials and tools

Materials	Tools
Bi_2O_3 (Merck) 99,99%	Digital scale
$SrCO_3$ (Merck) 99,99%	Mortar
PbO (Merck) 99,99%	Pestle
CuO (Merck) 99,99%	Hydraulic press
$CaCO_3$ (Merck) 99,99%	Furnace
Aceton	Crucible alumina

All starting materials in powder form were mixed and ground using a mortar and acetone as a wetting agent for 24 hours. The resulting homogeneous mixture was then pelletized using a cylindrical mold with a diameter of 1.5 cm under a pressure of 8 tonnes, yielding pellets with an average thickness of 1.7 mm.

Subsequently, the pellets were subjected to a calcination process at a heating rate of 600 °C per hour until reaching 810 °C, with a dwell time of 20 hours. The calcined samples were then sintered at a temperature of 846 °C for varying durations of 30, 32, and 34 hours. In this study, samples with sintering times of 32 and 34 hours are referred to as S32 and S34, respectively.

The microstructural properties of the samples were analyzed using X-ray diffraction (XRD), scanning electron microscopy (SEM), and energy-dispersive X-ray spectroscopy (EDX). XRD analysis was performed using a Shimadzu D6000 diffractometer, operated in continuous scanning mode over a 2θ range of 10° to 80°, using CuKα radiation (λ = 1.54060 Å) at 40 kV and 30 mA. The resulting diffraction patterns were compared with standard reference spectra of the BSCCO-2223 phase to identify the crystalline phases and evaluate phase purity.

Surface morphology, elemental composition, and pore structures were characterized using a JEOL JSM-6510LV SEM equipped with an EDS detector. Mechanical properties were assessed via Vickers microhardness testing, using a digital microhardness tester model HWDM3 at room temperature (25 °C). A load of 0.2 kgf was applied to the sample surface with a dwell time of 10 seconds, in accordance with ASTM E92.

4. Result and Discussion

4.1. The X- Ray Diffraction (XRD) Analysis

The X-ray diffraction (XRD) patterns of all samples are presented in Fig. 2a and 2b. Each pattern illustrates the relationship between the diffraction angle (2θ) and the intensity of the diffraction peaks. The results of the XRD pattern identification calculations for all samples are shown in Table 2. These peaks result from the reflection of X-rays by the crystal planes, which are identified by specific Miller indices (hkl). In Fig. 2a and Fig. 2b peaks labeled with hkl values correspond to the desired ceramic composite phase, while unlabeled peaks represent impurity phases. The presence of diffraction peaks with hkl indices of the form (00l), where *l* is an even number, indicates a degree of preferred orientation within the target phase formed in the samples.

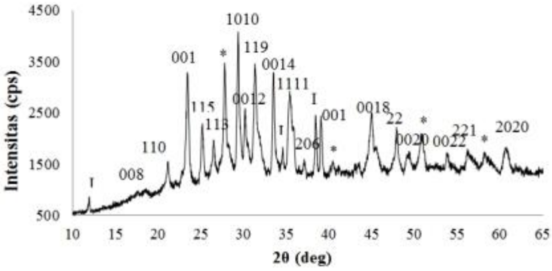

Fig 2a. XRD spectrum results from sample S32 with a sintering time of 32 hours

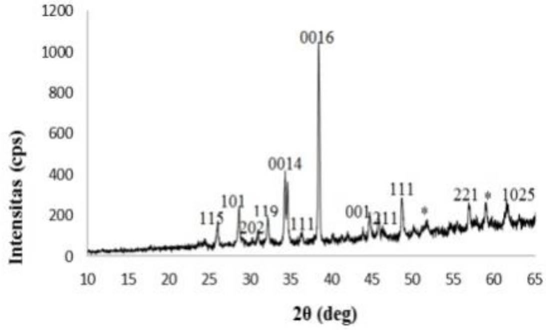

Fig 2b. XRD spectrum results from sample S34 with a sintering time of 34 hours

Table 2. The results of the XRD pattern identification calculations for all samples

Sample code	Sintering time (hours)	Volume fraction FV (%)	Impurity I (%)	Oriented phase P (%)	Average diameter D (nm)
S32	32	78.19	21.81	44.70	26.11
S34	34	93.95	6.05	58.12	48.07

As shown in Table 2, increasing the sintering time from 32 to 34 hours significantly affected the microstructural development of the material samples in this study. On average, the sample sintered for 34 hours (S34) exhibited improved crystal grain structure quality, with a larger grain size reaching up to 48.07 nm. The impurity content was also lower in the S34 sample, at only 6.05%. The formation of impurities is often unavoidable, as even a pure substance with a precise stoichiometry may exhibit more than one crystalline solid phase. However, only one phase tends to be thermodynamically stable under specific environmental conditions [14]. A solid phase may transform into another when subjected to changes in temperature or pressure, shifting into the stability field of the new phase and facilitating thermodynamic equilibrium [15]. Furthermore, the type of furnace used can influence the material's characteristics by affecting the oxygen exchange process and carbonate evaporation during sintering [16]. XRD analysis also revealed that sintering duration influences crystal growth. In the sample subjected to prolonged sintering (S34), crystal grains underwent significant growth, resulting in larger grain sizes. If the sintering temperature employed is not optimal, excessive crystal growth may occur, potentially leading to grain sizes in the micrometer range [17]. During the extended holding time, the grains undergo a recovery process in which they reorganize to minimize defects and develop a denser microstructure. At this stage, grain boundaries come into close proximity and may coalesce, indicating that sintering time also impacts both crystal size and sample porosity [18].

4.2. The Scanning Electron Microscopy (SEM) Analysis

The microstructural and elemental characteristics of the samples were further examined using SEM/EDX analysis, as illustrated in Fig. 3a and 3b. SEM observations revealed that the crystal grains possess a sheet-like morphology and are arranged in a random orientation [19]. Several types of grain boundary surfaces were identified, with noticeable voids between grains, indicating a need for further microstructural optimization.

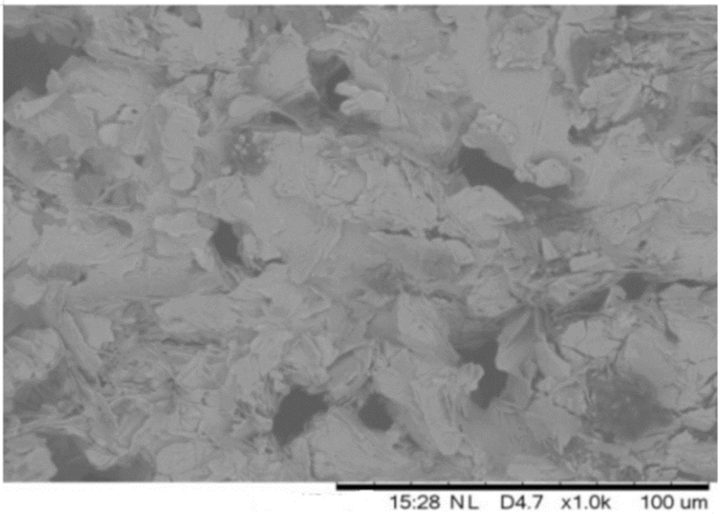

Fig 3a. SEM results of S32 sample with a sintering time of 32 hours

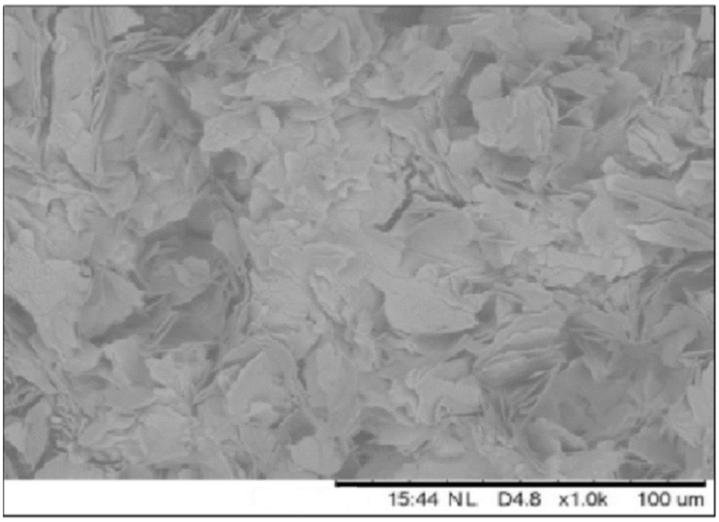

Fig 3b. SEM results of S34 sample with a sintering time of 34 hours

4.3. The Energy Dispersive X-ray Spectroscopy (EDX) Analysis

The EDX results confirmed the presence of chemical elements consistent with the expected 2:2:2:3 stoichiometric ratio, as illustrated in Fig. 4a and 4b.

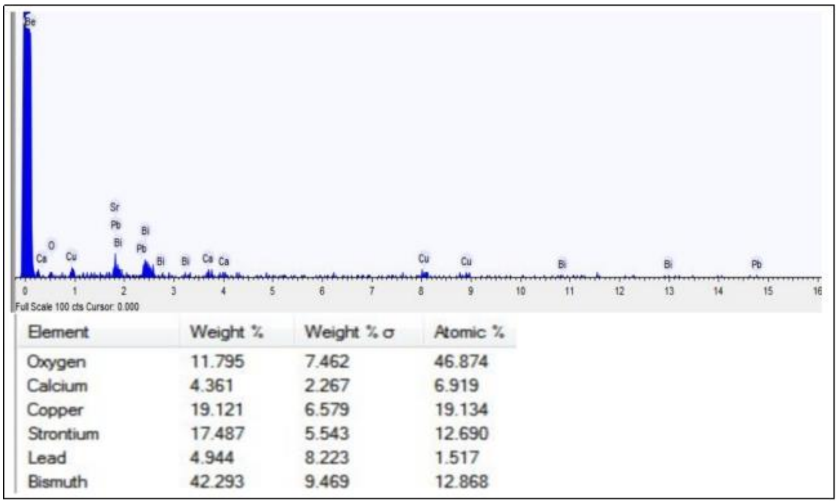

Element	Weight %	Weight % σ	Atomic %
Oxygen	11.795	7.462	46.874
Calcium	4.361	2.267	6.919
Copper	19.121	6.579	19.134
Strontium	17.487	5.543	12.690
Lead	4.944	8.223	1.517
Bismuth	42.293	9.469	12.868

Fig 4a. The EDX results of S32 sample with a sintering time of 32 hours

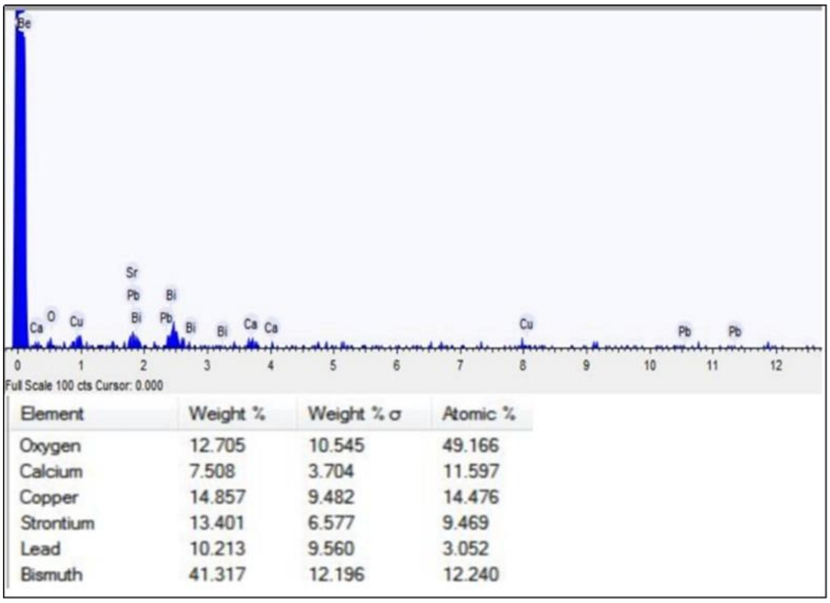

Element	Weight %	Weight % σ	Atomic %
Oxygen	12.705	10.545	49.166
Calcium	7.508	3.704	11.597
Copper	14.857	9.482	14.476
Strontium	13.401	6.577	9.469
Lead	10.213	9.560	3.052
Bismuth	41.317	12.196	12.240

Fig 4b. The EDX results of S34 sample with a sintering time of 34 hours

4.4. The Microhardness Vickers (HV) Analysis

All samples with codes S32 and S34 were subjected to the Vickers microhardness test. The results of mechanical property calculations for all samples are shown in Table 3. It can be seen that the Vickers number for the sample code S32 with a sintering time of 32 hours is 0.905, while the Vickers number for the sample with a sintering time of 34 hours (code S34) is 0.925.

Table 3. The mechanical properties for all samples

Sample code	Sintering time (hours)	Vickers number (GPa)	Yield strength	Young's modulus	Fracture Toughness	Surface energy(J)	Britleness index
S32	32	0.905	0.301	74.200	5.170	0.180	0.175
S34	34	0.925	0.308	75.813	5.200	0.178	0.177

Samples S32 and S34 successfully withstood the applied load; however, indentation marks from the diamond indenter were observed on the surface of the test specimens. These indentation traces reflect the material's response to three key microstructural properties: (i) crystal grain structure, (ii) grain orientation, and (iii) intergranular porosity [20]. The Vickers hardness value of sample S34 was higher than that of S32, indicating a denser microstructure with reduced porosity. An increase in hardness generally implies a decrease in porosity [21], which is further supported by the SEM images of the sample (Fig. 3b). The extended sintering duration of 34 hours for sample S34 positively influenced its hardness compared to sample S32, which was sintered for only 32 hours.

Several factors influence the hardness (Vickers number), including the initial processing conditions, calcination and sintering temperatures, and the duration of thermal treatment. During sintering, grains undergo a recovery process in which they rearrange to minimize defects and form a denser structure. As grain boundaries come into closer proximity, they may merge, reducing porosity and enhancing mechanical strength [22]. A higher Vickers hardness value reflects improved mechanical performance but also corresponds to an increase in the brittleness index, making the material more susceptible to fracture under impact loads [23].

The mechanical properties of the samples are summarized in Table 3. Sample S34 exhibited a Young's modulus of 75.813 GPa, slightly higher than that of S32 (74.20 GPa). The Young's modulus of the composite is the ratio between the stress with a strain that occurs [24]. The yield strength of S34 was 0.308 GPa, compared to 0.301 GPa for S32. The fracture toughness values were 5.2 for S34 and 5.17 for S32. The lowest surface free energy was recorded for S34 at 0.178 J, slightly lower than S32's value of 0.18 J. The brittleness index was marginally higher for S34 (0.177) compared to S32 (0.1775). These results suggest that while S34 demonstrated higher hardness, it also exhibited slightly increased brittleness.

Overall, the Vickers hardness value plays a critical role in determining the micromechanical behavior of the material. As presented in Table 3, the sintering holding time significantly affects the hardness, primarily due to the continuous formation of new grain boundaries and the coalescence of grains during prolonged heat treatment [25]. Extended sintering promotes particle mobility and grain vibration, especially in Bi-2223 phase materials, facilitating grain growth [26]. If the sintering temperature exceeds the optimal value, the grain size may become excessively large, potentially reaching the micrometer scale. Conversely, if the temperature is insufficient, the target phase may remain underdeveloped or be accompanied by significant impurity phases [27].

During sintering, the grains undergo a self-restructuring process that reduces crystal defects by forming a denser and more unified grain structure [28]. The resulting larger grains help minimize weak grain boundary connections, which is essential for enhancing currentcarrying capacity in power transmission applications [29]. Superior micromechanical properties are therefore advantageous and desirable for practical superconducting applications.

5. Conclusion

The results of this study demonstrate that the physical and mechanical properties of the material improve with increased sintering time. A holding time of 34 hours at the maximum sintering temperature yielded superior enhancements in both the microstructure and mechanical characteristics of the Bi-2223 ceramic composite samples compared to a holding time of 32 hours. SEM analysis showed layered grain structures, with some oriented along crystallographic planes. However, the presence of pores between grain boundaries suggests that further optimization of the synthesis process is necessary. EDX results confirmed the successful formation of the target 2:2:2:3 phase composition in all BSCCO samples. XRD analysis indicated that the largest grain size, 48.07 nm, was observed in the sample sintered for 34 hours. This sample also exhibited the highest percentage of oriented phase (58.12%) and the lowest impurity content (6.05%), highlighting its superior microstructural properties compared to the sample sintered for 32 hours. These features make the S34 sample more suitable for power transmission applications. Mechanical testing using Vickers microhardness measurements revealed that the S34 sample achieved the best performance, with a Vickers hardness of 0.905 GPa, Young's modulus of 74.2 GPa, yield strength of 0.301 GPa, fracture toughness of 5.17, surface energy of 0.180 J, and a brittleness index of 0.177. These mechanical properties, achieved through extended sintering, are advantageous for the development of high-performance superconducting wire materials. Future studies should focus on a more detailed and systematic investigation to determine the optimal sintering time for achieving bismuth-based ceramic composites with enhanced structural integrity and superior functional performance.

References

[1] G. Vadakkathillam, "Evolution of Superconducting Properties of Coexistent Bi-2212 and Bi-2223 phases in BSCCO," Indian J. Pure Appl. Phys., no. May, 2021.

[2] A. C. Mark et al., "Structure and equation of state of Bi2Sr2Can-1Cun O2n+4+δ from x-ray diffraction to megabar pressures," Phys. Rev. Mater., vol. 7, no. 6, 2023.

[3] A. N. S. Al Azzawi, M. B. Türköz, Ü. Erdem, and G. Yildirim, "Improvement in organization of Cu–O coordination and super-electrons in Bi-2212 ceramic matrix with Ag/Sr partial substitution," J. Mater. Sci. Mater. Electron., vol. 35, no. 18, pp. 1–25, 2024.

[4] A. R. Abdulridha, E. Al-Bermany, F. S. Hashim, and A. H. Omran Alkhayatt, "Synthesis and characterization and pelletization pressure effect on the properties of Bi1.7Pb0.3Sr2W0.2 Ca2Cu3 O10+δ superconductor system," Intermetallics, vol. 127, no. October, p. 106967, 2020.

[5] N. Ayai et al., "Progress in performance of DI-BSCCO family," Phys. C Supercond. its Appl., vol. 468, no. 15–20, pp. 1747–1752, 2008.

[6] P. K. Verma, T. Rajasekharan, S. C. Das, K. P. Surendran, and V. Seshu Bai, "Effect of nano ZrO2addition on the properties of Ca0.86Sr0.14CuO2added Bi 2223 composites," J. Phys. Conf. Ser., vol. 2545, no. 1, 2023.

[7] L. Opirina, A. Azwanda, and R. Febrianto, "Analysis of The Mechanical Properties of Concrete Based on Fly Ash and Palm Oil Clinkers," *International. J.ournal Engineering, Sci.ence and Inf.ormation Technol.ogy*, vol. 1, no. 4, pp. 31–35, 2021.

[8] N. K. Saritekin and A. T. Üzümcü, "Improving Superconductivity, Microstructure, and Mechanical Properties by Substituting Different Ionic Pb Elements to Bi and Ca Elements in Bi-2223 Superconductors," J. Supercond. Nov. Magn., vol. 35, no. 9, pp. 2259–2273, 2022.

[9] J. M. Costa, B. S. Monteiro, F. A. Rocha, M. S. Cunha, M. F. Vieira, and E. W. Sequeiros, "The Heat Treatment Effects on the Microstructure, Hardness, and Sigma Phase Content of L-PBF SAE 316L Stainless Steel," Acad. Mater. Sci., pp. 1–10, 2024.

[10] N. S. Farghal, A. Abu Shamleh, O. Al Hurmuzi, and O. Mahmoud, "The effects of a carbonated beverage on the optical properties and microhardness of preheated bulk-fill composite resin restorations," Front. Oral Heal., vol. 6, no. June, 2025.

[11] R. J. C. Batista et al., "Nanomechanics of few-layer materials: do individual layers slide upon folding?," Beilstein J. Nanotechnol., vol. 11, no. December, pp. 1801–1808, 2020.

[12] M. S. Hassan, I. E. Mohamed, M. Matar, A. I. Abou-Aly, R. Awad, and M. Anas, "Effect of hard magnetic ferrite (Ba0.5Sr0.5Fe12O19) nanoparticles on the mechanical properties of the (Bi, Pb)-2223 phase," Appl. Phys. A Mater. Sci. Process., vol. 129, no. 5, 2023.

[13] S. N. Abdullah et al., "Microstructure and Superconducting Properties of Bi-2223 Synthesized via Co-Precipitation Method: Effects of Graphene Nanoparticle Addition," Nanomaterials, vol. 13, no. 15, 2023.

[14] F. Haftlang and H. S. Kim, "A perspective on precipitation-hardening high-entropy alloys fabricated by additive manufacturing," Mater. Des., vol. 211, p. 110161, 2021.

[15] Y. Takeda, G. Nishijima, K. Inoue, Y. Takano, and H. Kitaguchi, "The effect of intermediate layer densification on the critical current of a Bi-2223 superconducting joint," Supercond. Sci. Technol., vol. 36, no. 3, p. 35004, 2023.

[16] D. V. Nichita, "A unified presentation of phase stability analysis including all major specifications," Fluid Phase Equilib., vol. 578, 2024.

[17] J. Zhang, "Oxygen Isotope Fractionation between Carbonate Minerals and Carbonic Acid Systems and Constraints for Environmental Science and Geological Processes," Molecules, vol. 29, no. 3, 2024.

[18] H. A. Lutpi, H. Mohamad, T. K. Abdullah, and H. Ismail, "-Effect of sintering treatment time on the sintering behaviour and thermal shock resistance of Li2O-Al2O3-SiO2 glass-ceramics," J. Asian Ceram. Soc., vol. 9, no. 2, pp. 507–518, 2021.

[19] R. Casasola, J. M. Pérez, and M. Romero, "Surface and volume crystallization in fluorrichterite based glasses," J. Asian Ceram. Soc., vol. 8, no. 3, pp. 642–652, 2020.

[20] Z. Ma, J. Gao, X. Weng, S. Yang, and K. Peng, "Synthesis and mechanism of aluminum silicate mesoporous materials by F108 template," Mater. Sci. Pol., vol. 38, no. 4, pp. 566–576, 2020.

[21] E. Strzałkowska, “Morphology and chemical composition of mineral matter present in fly ashes of bituminous coal and lignite,” Int. J. Environ. Sci. Technol., vol. 18, no. 9, pp. 2533–2544, 2021.

[22] X. Du, R. Liu, X. Xiong, and H. Liu, “Effects of sintering time on the microstructure and properties of an Al-Cu-Mg alloy,” J. Mater. Res. Technol., vol. 9, no. 5, pp. 9657–9666, 2020.

[23] M. R. Mazlan et al., “Necking mechanism under various sintering process parameters – A review,” J. Mater. Res. Technol., vol. 23, no. February, pp. 2189–2201, 2023.

[24] R. Dewi, O. Oktaviani, Z. Ginting, and N. Sylvia, “Mechanical Characteristic and Water Absorption Property of Bio Composite from Sago Starch and Jute Fiber (Boehmeria Nivea) as the filler,” *International. J.ournal Engineering, Sci.ence and Inf.ormation Technol.ogy*, vol. 2, no. 1, pp. 94–99, 2021.

[25] T. Miura, K. Sato, and H. Nakamura, “Influence of primary cracks on static and fatigue compressive behavior of concrete under water,” Constr. Build. Mater., vol. 305, no. November 2020, p. 124755, 2021.

[26] J. Liang, H. K. Yang, X. Huang, L. Y. Gao, and Z. Q. Liu, “Revealing the Mechanical Properties and Fracture Mechanism of Ag Paste Sintered Solder by Two Different Preparation Methods,” Materials (Basel)., vol. 18, no. 7, pp. 1–15, 2025.

[27] Z. K. Alkaabi and E. K. Al-Shakarchi, “Effect of Sintering Temperatures on the Physical Properties of Bi-2223 System Prepared by Co-Precipitation Method,” Mater. Sci. Forum, vol. 1084, no. April, pp. 9–14, 2023.

[28] N. Q. Chinh, D. Olasz, A. Q. Ahmed, E. V. Bobruk, and R. Z. Valiev, “Review on Grain Size- and Grain Boundary Phenomenon in Unusual Mechanical Behavior of Ultrafine-Grained Al Alloys,” Mater. Trans., vol. 64, no. 8, p. MT-MF2022020, Aug. 2023.

[29] B. Akkurt, U. Erdem, Y. Zalaoglu, A. T. Ulgen, T. Turgay, and G. Yildirim, “Evaluation of crystallographic and electrical-superconducting features of Bi-2223 advanced ceramics with vanadium addition,” J. Mater. Sci. Mater. Electron., vol. 32, no. 4, pp. 5035–5049, 2021.